PERGAMON

International Journal of Solids and Structures 39 (2002) 3523–3541

INTERNATIONAL JOURNAL OF SOLIDS and STRUCTURES

www.elsevier.com/locate/ijsolstr

Static liquefaction of a saturated loose sand stratum

Claudio di Prisco *, Silvia Imposimato

Dipartimento di Ingegneria Strutturale, Politecnico di Milano, Piazza Leonardo da Vinci, 32-20133 Milano, Italy

Received 13 February 2002

Abstract

The ideal case of an infinite horizontal, homogeneous oedometrically consolidated saturated loose sand stratum, sheared in displacement controlled conditions is numerically analysed. The phenomenon of the stratum liquefaction, which is due to both the material mechanical instability and the water presence within pores, is discussed. The numerical results have been obtained by means of a spatial one dimension finite difference numerical code within which both the local and the non-local versions of the same elasto-viscoplastic constitutive model are implemented. Both pore water and shear strain wave propagation within the soil layer is described.

Keywords: Soil liquefaction; Numerical analysis; Elasto viscoplastic and non local constitutive modelling

1. Introduction

The problem of static liquefaction of loose sand is nowadays a classical soil mechanics subject. Since the earlier experimental results of Castro (1969), the volumetric instability which is observed during undrained triaxial tests was associated to the compactant mechanical response of such materials. When the compaction is prevented by the presence of water within the intergranular voids, the pore pressure increases and the effective mean pressure decreases. Liquefaction takes place when the effective mean pressure becomes zero. From a mechanical point of view, the soil liquefaction is anticipated by an unstable mechanical response which will be better clarified in the following (Nova, 1991). Fully undrained tests may be easily performed in the laboratory, but, because of the high values of the sand permeability coefficient, when boundary value problems are taken into consideration, it is difficult to imagine such a condition to be satisfied.

When boundary value problems are analysed, sand behaves always in partially drained conditions and an important role is played by the time: i.e. by the coefficients or functions which describe the dependency of variables on the time factor. These are, for instance, the permeability and viscosity constants and the external loading rate.

The impulse to study from a mechanical point of view static liquefaction derives from the enormous economical importance of the consequences of natural phenomena induced by such volumetric instabilities.

* Corresponding author. Fax: +39-2-2399-4220.
E-mail address: cdiprisc@stru.polimi.it (C. di Prisco).

0020-7683/02/$ - see front matter
PII: S0020-7683(02)00164-6

Underwater slides, causing disastrous consequences, are very common all around the world. As reported by Terzaghi (1957), Andersen and Bjerrum (1968), Sladen et al. (1985), Kramer and Seed (1988) and many other authors, failures may occur both in artificial deposits either earth dams or hydraulically filled submarine berms and along marine or lacustrine shores. The factors, which affect the safety of these natural or artificial slopes, are manifold: large earthquakes, micro-seismic phenomena, local seepage, rapid variation of tide level, rapid accumulation of sediments and many others. Collapses take place instantaneously, slope inclinations may be very gentle and the volume of material moved enormous.

Displacement controlled ideal shear tests will be numerically analysed. Different versions of the same constitutive model have been implemented: an elasto-viscoplastic and a non-local elasto-viscoplastic one.

In the case of the elasto-viscoplastic version, different definitions for the viscous nucleus will be introduced and the numerical consequences of these choices discussed.

The mechanical meaning of the analysed instability will be clarified by prevently discussing some already published numerical results obtained by implementing the elasto-plastic version of the model.

2. Constitutive modelling

2.1. Undrained loose sand mechanical behaviour

In the last few decades, an enormous amount of experimental results concerning the static liquefaction of loose sands have been published. Three distinct ingredients have been considered to be necessary for liquefaction to occur: the soil specimen saturation, the undrained conditions and the material low relative density (Ishihara, 1993). As is schematically shown in Fig. 1, where experimental curves are plotted in the triaxial planes q–p' and q–ε ($q = \sigma_a - \sigma_r$, $p' = (\sigma'_a + 2\sigma'_r)/3$, $\varepsilon = 2/3(\varepsilon_a - \varepsilon_r)$), $\sigma'_{ij} = \sigma_{ij} - u\delta_{ij}$, where δ_{ij} is the Kronecker tensor, u is the pore pressure, small "a" stands for axial and small "r" for radial and, according to geotechnical conventions, compression is assumed to be positive), when strain controlled undrained standard compression triaxial tests are performed on isotropically consolidated loose sand specimens, a marked peak in the q value is observed. Moreover, even if, after the peak, q decreases, the stress level η ($\eta = q/p'$) continues to increase.

By following Lade (1992) the straight line, which passes through the peaks of the effective stress paths plotted in the triaxial q–p' plane, obtained by performing the same test on loose sand specimens isotropically consolidated at different effective mean pressures, may be defined as instability line. In the last ten years, many authors (Canou et al., 1991; di Prisco et al., 1995) have experimentally demonstrated that such

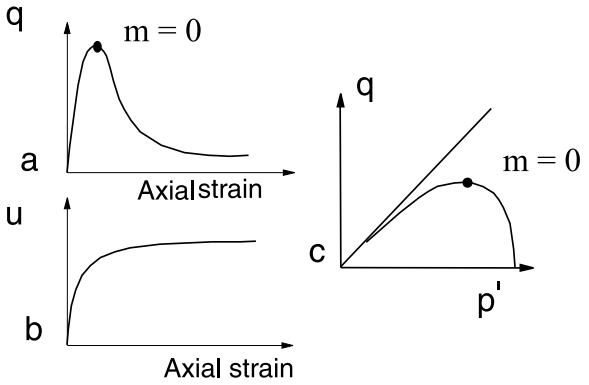

Fig. 1. Schematic representation of static liquefaction of very loose sand during standard triaxial undrained compression tests: (a) stress–strain curve, (b) pore pressure trend, (c) effective stress path.

a locus is dramatically influenced by the type of consolidation and by the previous strain history. Because of the induced anisotropy, it is possible to obtain a partially liquefiable behaviour even when a dense sand specimen is tested (Lanier et al., 1991).

2.2. Elasto-plastic modelling

If we want to reproduce the experimental results cited in Section 2.1 by means of a single potential strain hardening elasto-plastic constitutive model and by interpreting the soil specimen as an homogeneous macroelement characterised by a uniform distribution of stress and strain, it is necessary to use a non-associated flow rule, i.e. $f \neq g$ (where f stands for the yield locus and g for the plastic potential). In fact as was demonstrated by Nova (1991), the peak in the q–p' during undrained triaxial compression tests is necessarily associated to the following mechanical condition:

$$m = C_{ijhk}\delta_{ij}\delta_{hk} = 0, \tag{1}$$

where C_{ijhk} is the incremental elasto-plastic compliance tensor.

m can be zero or negative only and only if either $f \neq g$ or $H < 0$, where H is the hardening modulus. di Prisco et al. (1995) experimentally demonstrated that when the undrained peak in the q–p' plane takes place, H is still positive; in fact, if an undrained compression triaxial test is experimentally performed up to the peak and at that stress level the drainage valve is opened, an hardening response is observed.

By summarising this latter result and the previous experimental observation about the dependency of the instability line on the material strain history, two ingredients are necessary to reproduce the mechanical response of loose sand specimens loaded in undrained conditions by means of a single potential strain hardening elasto-plastic constitutive model:

- the non-associativeness,
- the anisotropic strain hardening.

Both the elasto-plastic and the elasto-viscoplastic versions of the constitutive model, which will be used in the following, satisfy both the above conditions and, as is shown in di Prisco et al. (1995), are capable to reproduce in undrained triaxial conditions the loose sand specimen liquefaction quite well. It is about of a single potential anisotropic strain hardening elasto-plastic constitutive model conceived in Milan and its detailed description is in di Prisco et al. (1993) but its main features are summarised in Appendix A. As far the elastic constitutive relationship is concerned, the Lade and Nelson model (1987) was implemented. The number of constitutive parameters is quite large (9 are plastic and 3 elastic), but their calibration may be performed by using very standard compression and extension triaxial tests.

By using the constitutive model as an heuristic tool, we can now imagine to perform, by imposing different boundary conditions and kinematic constraints, some less standard numerical tests. We can consider, for instance, the mechanical problem of an ideal infinitely extended loose sand layer which is sheared uniformly in undrained conditions and, in particular, we can take into consideration a soil element placed at a certain depth ξ. In this case all the terms of the strain rate tensor are nil except for the shear strain rate $\gamma_{\xi\eta}$ (Fig. 2).

If we perform such a theoretical test by using the previously cited constitutive model with the constitutive parameters calibrated thanks to the experimental results obtained by performing triaxial tests on very loose sand specimens, we obtain the curves schematically illustrated in Fig. 3 (di Prisco et al., 1995). The evident marked peak corresponding to the undrained test is analogous to that of Fig. 1, but in this case mechanical condition (1) is meaningless and must be substitute with the following one

$$D_{\xi\eta\xi\eta} = 0, \tag{2}$$

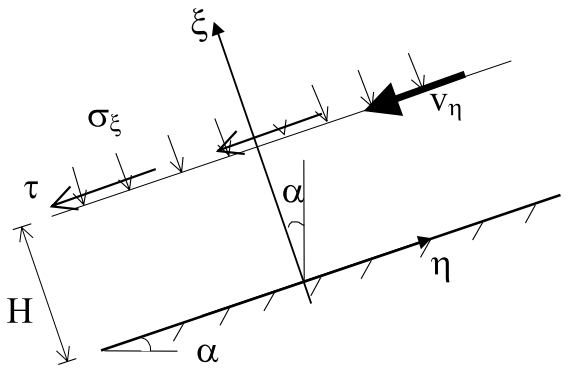

Fig. 2. Schematic geometrical representation of the problem considered.

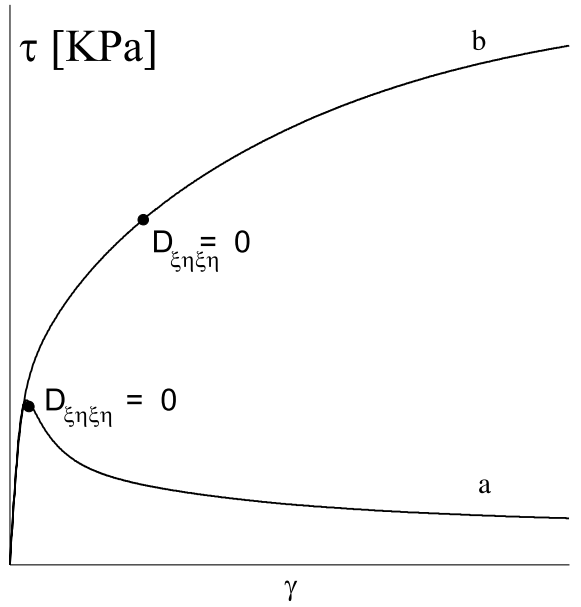

Fig. 3. Schematic representation of two ideal strain controlled shear test on a loose sand element volume: ($\alpha = 0^{\circ}$); curve a: undrained test, curve b: drained test.

where $D_{\alpha\beta\gamma\delta}$ is the incremental elasto-plastic stiffness tensor, while the axes ξ and η are those plotted in Fig. 2. When drained shear tests are performed, $D_{\xi\eta\xi\eta}$ can change sign but no mechanical consequences derive (curve b of Fig. 3).

2.3. Elasto-viscoplastic modelling

An elasto-plastic constitutive model implicitly assume that the mechanical response of the material to any static perturbation is instantaneous: i.e. any time dependency of the mechanical behaviour is disregarded. On the contrary, it is obvious that any microstructural evolution associated to the occurrence of irreversible strain increments must take place with time: it is only a question of time scale (di Prisco and

Imposimato, 1996). When loose sands are considered, the time period during which the system evolution takes place is small, in comparison with clays, for instance, but not nil. In particular, such a time dependency cannot be neglected when unstable phenomena take place, because in this case the phenomenon time scale changes abruptly.

A simple method to demonstrate, that such a time dependency of the mechanical behaviour of loose sands exists, consists in performing standard triaxial both drained and undrained creep tests. It is interesting, on the contrary, to observe that, by performing standard strain controlled tests at variable strain rate, it is very difficult to notice the difference in the mechanical response.

If we want to reproduce the cited above time dependency of the loose sand mechanical behaviour by starting from a standard elasto-plastic model, a good choice consists in following the classical Perzyna's (1963) approach. The flow rule is modified as below and the consistency rule disappears:

$$\dot{\varepsilon}_{ij}^{\mathrm{vp}} = \Phi(f) m_{ij}, \tag{3}$$

where $\Phi(f)$ is the viscous nucleus, f is the yield function, m_{ij} is the gradient to the plastic potential and, as in Eqs. (5) and (8), the superimposed dot stands for partial time derivative. The elastic response is assumed to be instantaneous and only irreversible/viscoplastic strains take place with time. The viscous nucleus plays a dominant role; its definition is fundamental in describing the material mechanical response during the evolution of time. A suitable choice is the following, which was suggested by di Prisco and Imposimato (1996):

$$\Phi(p', f) = p' \widehat{\Phi}(f) = \bar{\gamma} p' \, \mathrm{e}^{\alpha f}, \tag{4}$$

where α and $\bar{\gamma}$ are constitutive parameters which describe the system evolution rate. Thanks to such a definition, the viscous nucleus is always positive, even when $f < 0$, i.e. when the effective stress state lies within the yield locus. As was shown in di Prisco et al. (1999) and di Prisco and Pastor (2000), such a peculiarity is experimentally supported by the mechanical behaviour of sand specimens during undrained q constant creep tests.

On the contrary, if we simulate strain controlled triaxial tests performed at variable strain rates, by means of a model which adopts such a highly non-linear definition for the viscous nucleus, we do not observe any time dependency of the soil mechanical behaviour neither in drained nor in undrained conditions. Moreover, when f is positive and continuously increases because of the occurrence of an unstable phenomenon, the viscous nucleus value tends quickly to infinite. For this reason, as it will be discussed more deeply in the following, it may be necessary, as schematically illustrated in Fig. 4, to introduce an upper bound for Φ, when f values are very large. Such a change does not induce any consequence on the simulated mechanical response in stable conditions, on the contrary in unstable conditions the numerical mechanical response may change dramatically (see Section 5). Unfortunately, according to the authors, an experimental calibration of such a limitation is difficult to be imagined.

As was done in di Prisco and Imposimato (in press) (Appendix B), a dependency of constitutive parameters on relative density is introduced, too. This allow us to reproduce the mechanical response of the material even when large volumetric strains take place. This is important when liquefaction takes place, because a sudden material compaction follows necessarily the material liquefaction.

Finally, we want to remind that, when a elasto-viscoplastic constitutive relationship is taken into consideration, we cannot associate to the undrained instability occurrence, simple and compact mathematical condition as Eqs. (1) and (2) are. In the case of elasto-viscoplastic models, the mechanical instability occurrence is coupled to an increase of f which is due to the rapid and sudden increase in pore pressure.

For this reason the phenomenon mechanical interpretation will be discussed by starting from the analysis of the numerical results obtained on a soil macro-element. The boundary value problem will be numerically solved by means of the elasto-viscoplastic version.

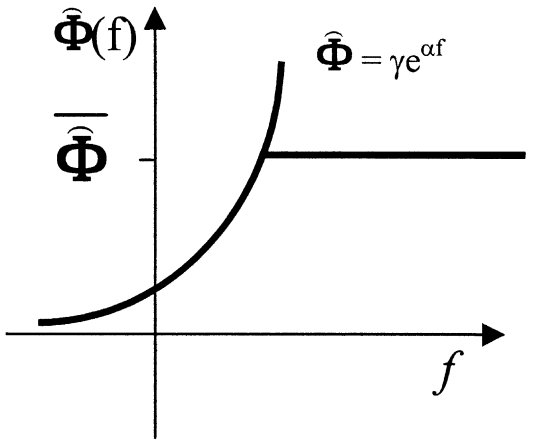

Fig. 4. Schematic representation of the viscous nucleus function: the exponential definition and the imposed upper bound.

2.4. Non-local elasto-viscoplastic constitutive model

A more sophisticated version of the constitutive model (di Prisco and Imposimato, in press) provides a non-local definition for Φ. Such a modification allows us to introduce a characteristic length in the model and to describe shear strain localisation phenomena. In Eqs. (5) and (6) the new definition for Φ is given:

$$\dot{\varepsilon}_{ij}^{\mathrm{vp}} = \Phi(\hat{f}) m_{ij}, \tag{5}$$

$$\hat{f} = \frac{\int_{\bar{V}} f(x_i)\mu(x_i)\,\mathrm{d}V}{\int_{\bar{V}} \mu(x_i)\,\mathrm{d}V}, \tag{6}$$

where μ is a bellshape function centred with respect to the point P relatively to which the value of $\hat{f}$ is calculated and $\bar{V}$ is a spherical volume which defines the spatial domain within which such a weight average is calculated. This becomes in one dimension:

$$\mu(x) = \frac{\mathrm{e}^{-(x-x_0)^2/2}}{\sqrt{2\pi}}, \tag{7}$$

where x_0 is the P coordinate. The only additional constitutive parameter is the value of the sphere radius R.

3. Boundary value problem description

In order to clarify from both a mechanical and a hydraulic point of view the static liquefaction phenomenon of saturated loose sands and to discuss whether the previously presented different constitutive approaches are capable, at least qualitatively, to simulate the experimental reality, a very simple geometrical boundary value problem was analysed. It is about an infinite homogeneous loose sand submerged stratum characterised by a variable inclination α, which is placed on a rigid sub-layer, whose position (H) is considered as a geometrical parameter of the problem. Because of symmetry conditions, all the functions

will depend only on the spatial variable (ξ). As far as boundary hydraulic conditions are concerned, the upper boundary is assumed to be permeable, while the lower one impervious.

This implies that the material locally behaves in partially drained conditions and a coupled geotechnical problem must be solved. The material has been assumed to obey to the Darcy's law; the permeability coefficient k_ξ is assumed to be constant along ξ and with time, even when liquefaction takes place. According to the authors, such a constraint represents the most unphysical condition imposed. In fact, during the liquefaction phenomenon, as suggested by Vardoulakis et al. (1998), the water flux cannot be considered as laminar and the Darcy's law should be abandoned.

The ideal soil layer may be tested both in load and displacement controlled conditions. In the former case both the normal stress σ_ξ and the shear stress $\tau_{\xi\eta}$ on the upper boundary are controlled. In the latter one, during the evolution of time, σ_ξ and the displacement along η are controlled.

As was observed in di Prisco et al. (in press), when a load controlled test is taken into consideration, the soil layer mechanical response can be described only up to the instability occurrence, but the solving mathematical system is incrementally uncoupled. In fact, because of the equilibrium equations, $\dot{\tau}_{\xi\eta}$ and $\dot{\sigma}_\xi$ are constant along ξ and consequently are known variables along ξ. The incremental solving equation is the continuity equation for the water flux. Thanks to this one, the increase in pore water pressure is calculated and consequently all the remaining stress and strain variable increments may be calculated.

When a displacement controlled test is analysed, the incremental mathematical system is coupled, because as above $\dot{\tau}_{\xi\eta}$ is constant along ξ but is unknown. The below coupled system must be incrementally solved:

$$\dot{v}_\eta(t) = \int_0^H \dot{\gamma}_{\xi\eta}(\xi, t)\,\mathrm{d}\xi, \tag{8a}$$

$$\dot{\gamma}_{\xi\eta}(\xi, t) = c_1(\xi, t)\dot{u}(\xi, t) + c_2(\xi, t)\dot{\tau}_{\xi\eta}(t) + c_3(\xi, t), \tag{8b}$$

$$\dot{u}(\xi, t) = a(\xi, t)\frac{\partial^2 u(\xi, t)}{\partial \xi^2} + b_1(\xi, t)\dot{\tau}_{\xi\eta}(t) + b_2(\xi, t). \tag{8c}$$

3.1. Mechanical observations

As was demonstrated in detail in di Prisco et al. (in press), where the problem of rapid sedimentation was considered as a triggering factor for the liquefaction to occur, when an elasto-plastic constitutive relationship is implemented, the numerical simulation of the volumetric instability cannot be reproduced. In fact, when condition (2) is fulfilled, coefficient a of Eq. (8c) becomes negative (Appendix C). When coefficient a becomes negative the spatial dissipative term (the first term right of Eq. (8c)) becomes a source term. In fact, where the sudden increase in pore pressure is recorded, the second derivative term with respect to ξ is negative and the previous observation derives.

In this case, as coefficient a may be written as follows:

$$a(\xi, t) = \frac{k_\xi}{\gamma_w} a^{\mathrm{ep}}(C^{\mathrm{ep}}_{ijhk}) \tag{9}$$

(where γ_w is the water unit weight and C^{ep}_{ijhk} is the incremental elasto-plastic compliance tensor), if we increased the permeability coefficient value, the increase in pore pressure would be more rapid. Naturally, it is evident that there is no physical sense in such a consequence.

Coefficient a becomes negative when $\dot{\tau}_{\xi\eta}$ is still positive and the peak is not yet reached. In fact, as previously underlined, Eq. (2) is a meaningful unstable condition only when undrained conditions are locally imposed, while Eqs. (8a)–(8c) were written to solve a coupled partially drained boundary value

problem. Of course, such a discrepancy disappears when $k_\xi \to 0$, but in this case undrained conditions are locally imposed.

When an elasto-viscoplastic constitutive model is numerically implemented, coefficient a is always positive because it is a principal minor of the elastic compliance tensor (Appendix D). When liquefaction takes place, term b_2, which is always nil in the elasto-plastic case, in the elasto-viscoplastic case increases rapidly and abruptly.

In fact, b_2 is defined as follows:

$$b_2 = b_2^*(C^{\mathrm{el}}_{ijhk}, m_{ij})\Phi(f), \tag{10}$$

where C^{el}_{ijhk} is the elastic compliance tensor. When liquefaction occurs, both f and Φ increase in a self feeding mechanism.

When the dissipative term does not balance the source term due to the viscoplastic compaction, the peak in the τ–γ plane is recorded. In this case, if we increased the permeability coefficient, we would prevent the liquefaction occurrence: the source term would be constant while the dissipative term would be increased. Numerical stability of Eq. (8c) is then linked to the evolution of term b_2 with time: b_2 may increase but its value must continue to be bounded. Eq. (10) shows clearly that the modulus of b_2 is strictly linked to both the viscous nucleus and the yield function definition.

When liquefaction occurs at a certain depth ξ, p' rapidly decreases, the yield function value increases and consistently the viscous nucleus value. All the function definitions are highly non-linear. If the increase in the Φ value is very rapid, the associated increase in pore water pressure and decrease in effective mean pressure induce a rapid increase in the f value, too. Because of the f and Φ chosen definition (Nova, 1988; di Prisco and Imposimato, 1996), as will be demonstrated numerically in the following paragraph, when liquefaction takes place, b_2 is unbounded and the propagation of the liquefaction phenomenon within the soil layer cannot be followed and the post peak regime cannot be reproduced.

In order to overcome such a problem, two different ways have been chosen: the former consists in modifying the viscous nucleus definition as was suggested in Section 2.3 (Fig. 4), the latter in adopting the non-local definition for Φ described in Section 2.4.

It is important to underline that the first choice is more direct and powerful because the Φ value is directly and artificially bounded. From a physical point of view, this means that the plastic strain rate may increase but will never become infinite. The second approach takes into account the spatial phenomenon diffusion. The non-local definition for Φ implies an average operation in a spatial domain. When liquefaction occurs at a certain point P, if Φ goes to infinite, a localisation phenomenon takes place and the surrounding points are not involved at all. This means that they will be unloaded. If we introduce a non-local approach, the average operation will allow the phenomenon propagation, because in P the non-local value will be reduced and, on the contrary, in the surrounding points it will increase.

The last factor which could induce a stabilizing effect would be the change in the rule which governs the water seepage within the porous continuum in order to take into account the turbulent phenomenon which takes place when the effective mean pressure rapidly decreases.

Such an aspect, for the sake of simplicity, has been here below completely disregarded and the permeability coefficient has been assumed to be constant during the test.

4. Numerical results

For the sake of simplicity, we will now illustrate some numerical results, which have been obtained by considering an infinite homogeneous horizontal loose Hostun RF sand layer ($\alpha = 0°$) subject to a dis-

placement controlled shear ideal test ($\dot{v}_\eta = \text{constant}$). The layer thickness $H = 0.5$ m. The layer is initially oedometrically consolidated under a vertical effective stress ($\sigma'_\xi = 100$ kPa), the initial pore pressure distribution is hydrostatic. The elasto-plastic material mechanical constitutive parameters were calibrated in di Prisco et al. (1995) while the two viscoplastic ones in di Prisco and Imposimato (1996) (Appendix E).

The constitutive model has been implemented in a finite difference numerical code. The time and spatial discretisation has been varied, but all the numerical results illustrated here below are independent of the mesh size.

The finite difference numerical scheme implemented is characterized by central differences in space and implicit integration in time.

In Fig. 5 the numerical results obtained by performing the ideal shear test described above are illustrated. In this case, the constitutive model is characterised by both a truncation of the Φ value (Section 2.3) and the non-local definition for Φ (Section 2.4). In particular, the maximum value for Φ has been assumed to be $\overline{\Phi} = 6$, while the radius $R = 0.015$ m. Finally, the imposed upper boundary displacement rate $\dot{v}_\eta$ has been assumed to be 0.00025 m/s and the permeability coefficient $k_\xi = 0.5 \times 10^{-6}$ m/s.

In Fig. 5a the global layer mechanical response is illustrated. The upper boundary horizontal displacement s_ξ is normalised by the total layer thickness H in order to give an average measure of the shear strain. It is evident the peak in τ ($\tau = \tau_{\xi\eta}$) and the subsequent strengthening due to the material consolidation.

In Fig. 5b the curves which describe the mechanical response at different depths are collected: the deepest point displacement ($\xi = H$) is negligible, the displacement field seems to be widespread along ξ. In fact, as is shown in Fig. 5c, relatively to the first one minute of test, and in Fig. 5e, relatively to the all test period, the shear strain γ ($\gamma = \gamma_{\xi\eta}$) is not localised at all, even if it is evident that the larger shear strains develop in the deeper part of the layer, as the upper part behaves in almost drained conditions. In Fig. 5c and e the shear strain wave propagation is illustrated. During the strengthening part of the curve plotted in Fig. 5a most shear strains develop, this is due to the persisting high values of excess pore pressure u^* for $\xi > H/2$ (Fig. 5d and f). It is important to observe that the final point of Fig. 5a, which was chosen because is characterised by a τ value equal to that one recorded at the peak, corresponds with an instant of time of 180 s. In Fig. 5f the 180 s isochronous curve is the curve characterised by the maximum value of excess pore pressure u^*.

In spite of the observed wave propagation, in these numerical analyses, dynamic forces are not taken into consideration. In fact, the acceleration terms are negligible. This is due to the fact that numerical tests are performed under displacement controlled conditions and along axis ξ, both the η and ξ displacement rates are approximately constant with time. In order to verify such an assumption, some numerical tests were performed by taking into account dynamic forces and no differences with respect to the previous numerical results were observed.

In Fig. 6, the analogous results obtained by analysing the same mechanical and hydraulic boundary value problem, with the same dimensions but with a different value of k_ξ ($k_\xi = 0.5 \times 10^{-5}$ m/s) are illustrated. In this case liquefaction does not occur, the mechanical response is stable. The pore pressure does not increase and any shear wave is not observable. Analogously, if we keep constant k_ξ ($k_\xi = 0.5 \times 10^{-6}$ m/s) and we decrease the upper boundary displacement rate, we obtain qualitatively the same numerical result. Here, for the sake of brevity, these numerical results are not reported.

It has been considered more interesting to analyse the effect of the two distinct constitutive modelling approaches introduced to regularise the numerical solution. First the effect of the truncation of Φ has been considered (Section 2.2). With respect to the previous case (Fig. 5) Φ is now a function of the local value of f. The observed numerical mechanical response is the same, both from a qualitative and a quantitative point of view.

On the contrary, if we numerically analyse the same problem by removing the non-local definition for Φ as above, but changing the maximum value for Φ ($\overline{\Phi} = 9$), as is shown in Fig. 7, the mechanical response remains unaltered up to the peak, but it changes markedly in the post peak regime.

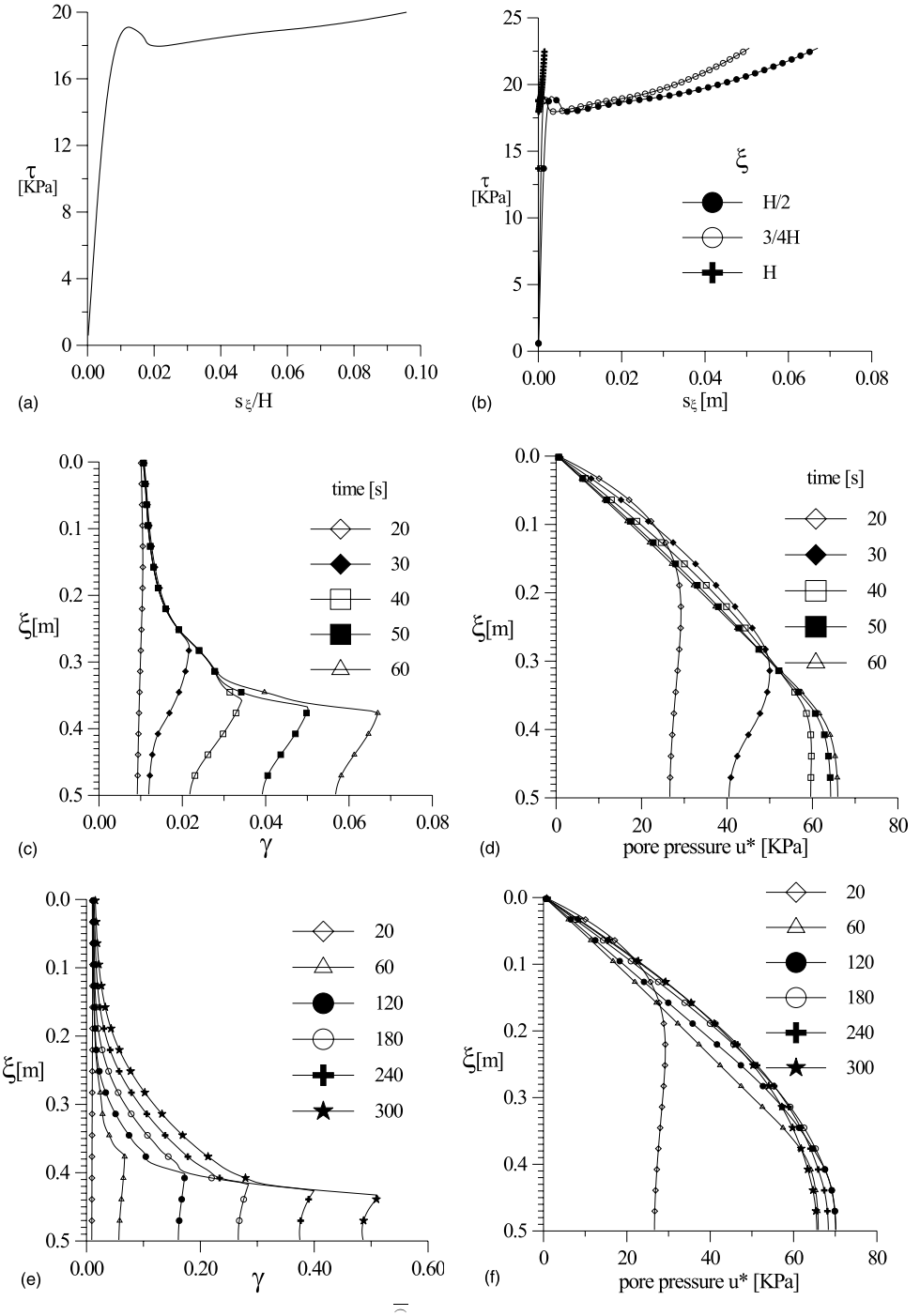

Fig. 5. Non-local elasto-viscoplastic constitutive model ($\bar{\Phi} = 6$), ideal partially drained displacement controlled shear test ($k_\xi = 0.5 \times 10^{-6}$ m/s) on an horizontal infinitely extended loose sand stratum: numerical simulations ($d\xi = 0.003$ m, $dt = 0.002$ s): (a) global mechanical response, (b) displacement field along the vertical axis ξ, (c) shear strain profile along ξ during the evolution of time (first 60 s), (d) excess pore water pressure along ξ during the evolution of time (first 60 s), (e) shear strain profile along ξ during the evolution of time (first 300 s), (f) excess pore water pressure along ξ during the evolution of time (first 300 s).

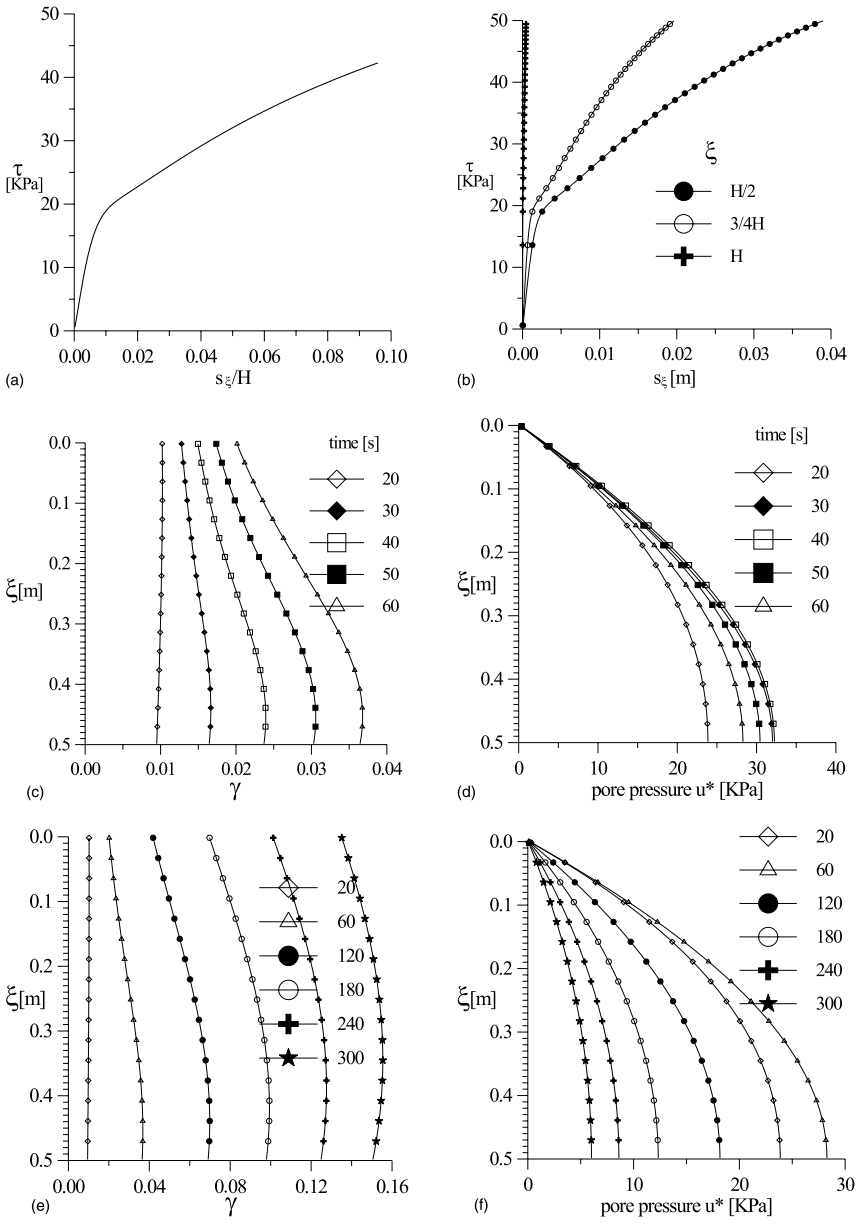

Fig. 6. Non-local elasto-viscoplastic constitutive model ($\overline{\widehat{\Phi}} = 6$), ideal partially drained displacement controlled shear test ($k_\xi = 0.5 \times 10^{-5}$ m/s) on an horizontal infinitely extended loose sand stratum: numerical simulations ($d\xi = 0.003$ m, $dt = 0.002$ s): (a) global mechanical response, (b) displacement field along the vertical axis ξ, (c) shear strain profile along ξ during the evolution of time (first 60 s), (d) excess pore water pressure along ξ during the evolution of time (first 60 s), (e) shear strain profile along ξ during the evolution of time (first 300 s), (f) excess pore water pressure along ξ during the evolution of time (first 300 s).

Finally, if we numerically analyse again the same problem by removing the constraint on the maximum value of $\widehat{\Phi}$ and by re-introducing its non-local definition ($R = 1.5$ cm), the mechanical response is qualitatively similar but quantitatively a bit different (Fig. 8). In particular some small oscillations are recorded

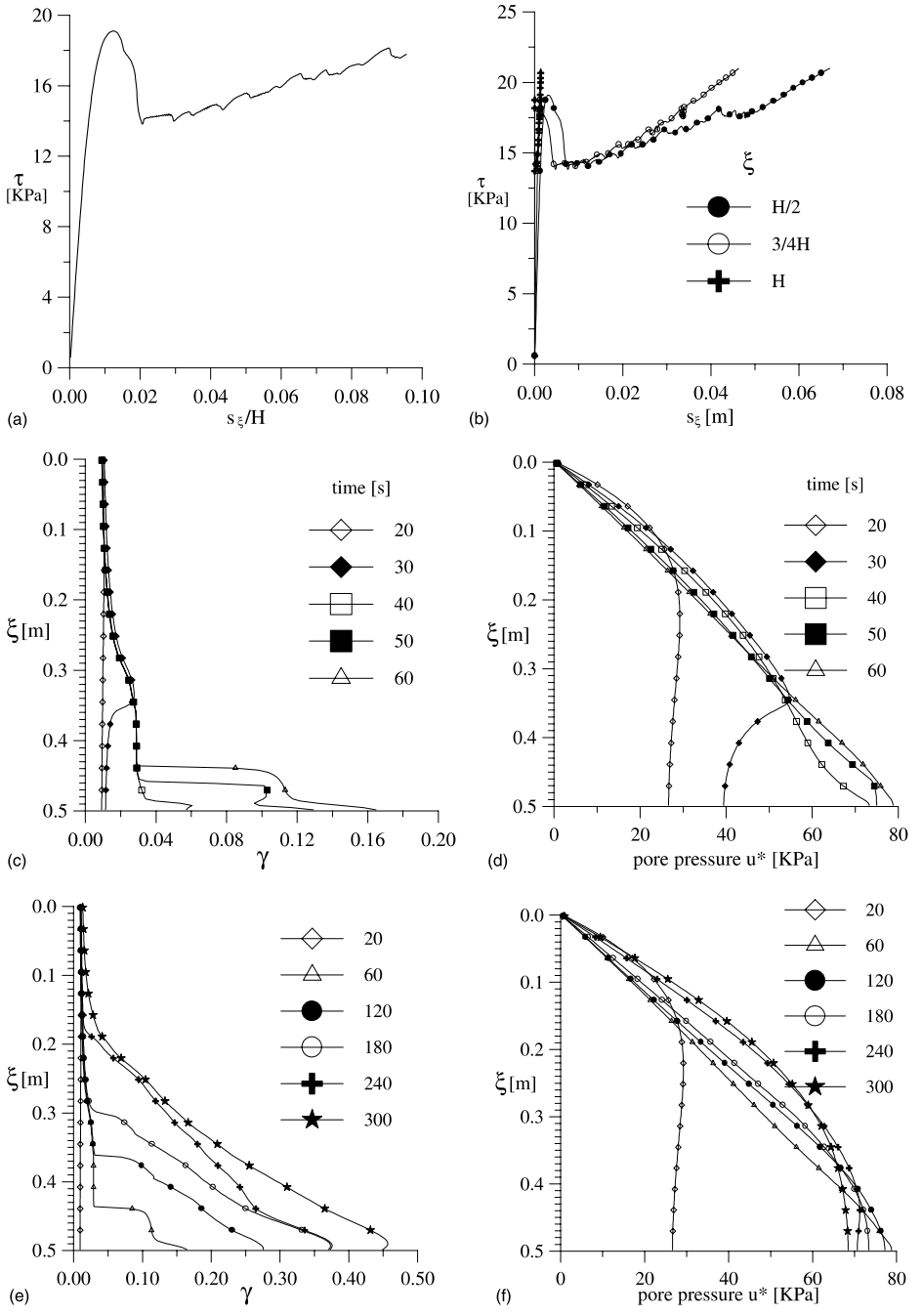

Fig. 7. Local elasto-viscoplastic constitutive model ($\widehat{\Phi} = 9$), ideal partially drained displacement controlled shear test ($k_\xi = 0.5 \times 10^{-6}$ m/s) on an horizontal infinitely extended loose sand stratum: numerical simulations ($d\xi = 0.003$ m, $dt = 0.002$ s): (a) global mechanical response, (b) displacement field along the vertical axis ξ, (c) shear strain profile along ξ during the evolution of time (first 60 s), (d) excess pore water pressure along ξ during the evolution of time (first 60 s), (e) shear strain profile along ξ during the evolution of time (first 300 s), (f) excess pore water pressure along ξ during the evolution of time (first 300 s).

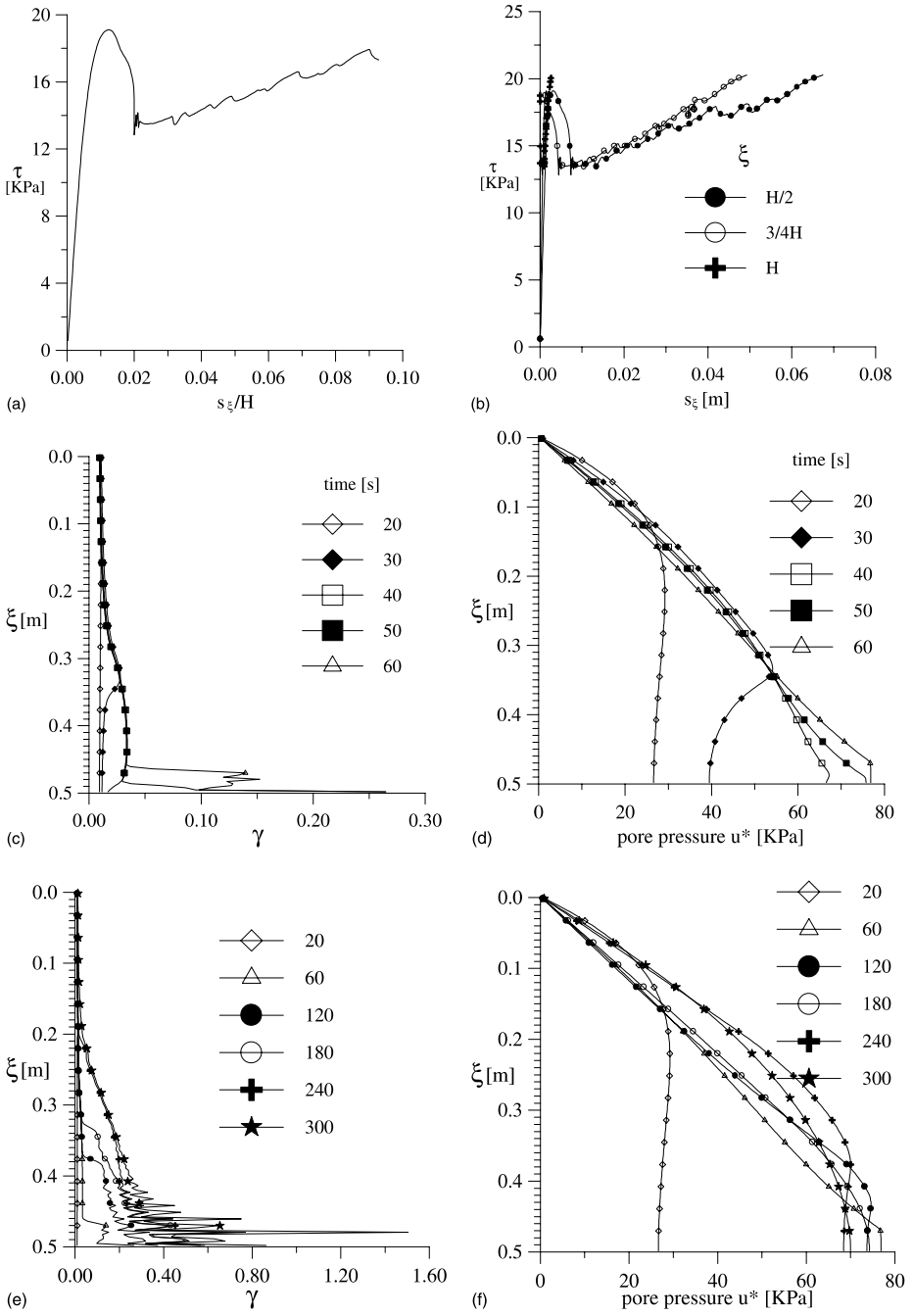

Fig. 8. Non-local elasto-viscoplastic constitutive model, ideal partially drained displacement controlled shear test ($k_\xi = 0.5 \times 10^{-6}$ m/s) on an horizontal infinitely extended loose sand stratum: numerical simulations (d$\xi = 0.003$ m, d$t = 0.002$ s): (a) global mechanical response, (b) displacement field along the vertical axis ξ, (c) shear strain profile along ξ during the evolution of time (first 60 s), (d) excess pore water pressure along ξ during the evolution of time (first 60 s), (e) shear strain profile along ξ during the evolution of time (first 300 s), (f) excess pore water pressure along ξ during the evolution of time (first 300 s).

in the γ versus ξ curves (Fig. 8c and e) but also in the global trend of Fig. 8a. These oscillations, analogous to those which may be observed in Fig. 7 where $\widehat{\Phi}$ is increased, are not linked to the time or spatial discretisation but only to the value of R.

5. Concluding remarks

The loose sand liquefaction phenomenon which takes place in partially drained conditions has been numerically simulated by means of an anisotropic strain hardening Perzyna's type viscoplastic constitutive model characterised by a non-associated flow rule. In particular a plane strain displacement controlled ideal shear tests performed on an infinite horizontal saturated stratum has been analysed.

Some numerical simulations of the liquefaction collapse propagation in a soil stratum were presented. The pore pressure as well as the shear strain wave propagation within the spatial and temporal domain were analysed. The importance of the loading rate as well as of the permeability coefficient was underlined. The instability occurs only when either the upper boundary displacement rate is sufficiently high or the permeability coefficient is sufficiently small. Naturally, the viscous nucleus definition, i.e. the constitutive parameters which define the time dependency mechanical behaviour plays an analogous role, but for the sake of simplicity these parameters were kept constant.

A discussion about the choice of the constitutive relationship was introduced. It was observed and mechanically explained that the elasto-plastic version of the model is not capable of reproducing the unstable phenomenon because of the instability of the continuity equation for the water flux. The original elasto-viscoplastic version is not adapt as well, because of both the yield function and viscous nucleus definition. When liquefaction takes place at a certain depth, the viscoplastic source term of the continuity equation for the water flux goes to infinite.

Two ways to avoid numerical instabilities were discussed: the non-local approach and a bounded definition for the viscous nucleus. Without any doubt, the latter seems to be more adapt, as the constraint is more strict. Unfortunately, the value of the imposed upper bound for the viscous nucleus, when liquefaction occurs, influences the system mechanical response and it is difficult to conceive an experimental method to calibrate it.

Three distinct phases of the phenomenon appear evident: (a) the pre-peak stable regime, (b) the unstable post-peak regime which is associated to the soil densification, (c) the final stable branch during which the pore water pressure generated by the material collapse is dissipated, the relative density as well as the shear stress increase.

Acknowledgements

This research was funded by the Italian CNR and MURST. The authors would like to acknowledging. P. Galvanin for having begun toddling in the right direction, Prof. R. Nova, Prof. M. Pastor and Prof. I. Vardoulakis for their precious observations.

Appendix A

The cited paper (di Prisco et al., 1995) introduces an elasto-plastic constitutive model which is the extension of Sinfonietta Classica constitutive relationship conceived by Nova (1988) to reproduce sand mechanical behaviour. An anisotropic strain hardening is assumed in order to capture the mechanical consequences of the induced anisotropy on the mechanical behaviour of granular soils.

Both the yield locus f and the plastic potential g evolve according to the strain history:

$$f = f(\sigma'_{hk}, \chi_{rs}, r_c, \beta_f), \tag{A.1}$$

$$g = g(\sigma'_{hk}, \chi_{rs}), \tag{A.2}$$

where χ_{rs} is a state variable tensor, while r_c and β_f are scalar state variables. χ_{rs} describes the rotation of the yield locus, r_c its size and β_f its shape.

The rotation of f and g is obtained by defining both the loci as functions of convenient tensorial variables η^*_{hk}:

$$\eta^*_{hk} = \frac{\sqrt{3}(\sigma'_{hk} - r\chi_{hk})}{r}, \tag{A.3}$$

where $r = \sigma'_{rs}\chi_{rs}$.

The complete definition for f and g are written here below:

$$f = 3\beta_f(\gamma - 3)\ln\frac{r}{r_c} - \gamma J_{3\eta^*} + \frac{9}{4}(\gamma - 1)J_{2\eta^*} \tag{A.4}$$

and

$$g = 9(\gamma - 3)\ln\frac{r}{r_g} - \gamma J_{3\eta^*} + \frac{9}{4}(\gamma - 1)J_{2\eta^*}, \tag{A.5}$$

where γ is a constitutive parameter, while

$$J_{2\eta^*} = \eta^*_{ij}\eta^*_{ij}, \tag{A.6}$$

and

$$J_{3\eta^*} = \eta^*_{ij}\eta^*_{jk}\eta^*_{ki} \tag{A.7}$$

as only the gradient tensor of g is used, r_g is not defined.

As far as the definition of the hardening rules is concerned, we can summarise as follows:

$$\dot{r}_c = \frac{r_c}{B_p}\left(\sqrt{3}\dot{\varepsilon}^p_{rs}\chi_{rs} + \xi\sqrt{\dot{e}^{p^*}_{rs}\dot{e}^{p^*}_{rs}}\right), \tag{A.8}$$

where B_p is a constitutive parameter which may be easily calibrated by means of isotropic compression tests. ξ is defined as a function of two constitutive parameters (ξ_c and ξ_e) according to a rule which is not described here in the following for the sake of brevity,

$$\dot{e}^{p^*}_{rs} = \dot{\varepsilon}^p_{rs} - \dot{\varepsilon}^p_{ij}\chi_{ij}\chi_{rs}, \tag{A.9}$$

$$\dot{\beta}_f = t_p(\hat{\beta}_f - \beta_f)\frac{\dot{e}^p_{rs}e^p_{rs}}{\sqrt{e^p_{rs}e^p_{rs}}}, \tag{A.10}$$

where t_p and $\hat{\beta}_f$ are constitutive parameters.

The hardening rule for χ_{rs} is more complex but may be outlined as follows:

$$\dot{\chi}_{ij} = \dot{k}(\hat{\chi}_{ij} - \chi_{ij}\chi_{rs}\hat{\chi}_{rs}), \tag{A.11}$$

where

$$\dot{k} = c_p\sqrt{\dot{\varepsilon}^p_{rs}\dot{\varepsilon}^p_{rs}}, \tag{A.12}$$

c_p is a constitutive parameter and $\hat{\chi}_{rs}$ is a limit tensor for χ_{rs} which is a function of η^*_{hk} and of two constitutive parameters $(\hat{\theta}_c, \hat{\theta}_e)$.

Appendix B

All the current elasto-plastic constitutive parameters p_i are assumed to depend on the current relative density D_r. In order to define such a dependency a linear interpolation was suggested between two different sets of parameters which will be collected in Tables 1 and 2 of Appendix E. The first set (p_{Di}) was calibrated on the mechanical behaviour of a very dense sand, ($D_r = 100\%$), the second one (p_{Li}) on the mechanical behaviour of a very loose Hostun RF sand ($D_r = 20\%$):

$$p_i = p_{Li} + (p_{Di} - p_{Li})D_r. \tag{B.1}$$

Appendix C

In the elasto-plastic case, when loading phase is considered, the coefficient of Eqs. (8a)–(8c) become (in all the following definitions, it is very important to underline, C_{ijhk} must be read as C^{ep}_{ijhk}) :

$$c_1(\xi,t) = -2(\tilde{C}_1 C_{1311} + \tilde{C}_3 C_{1322} + C_{1333}), \tag{C.1}$$

$$c_2(\xi,t) = 4(\tilde{C}_2 C_{1311} + \tilde{C}_4 C_{1322} + C_{1313}), \tag{C.2}$$

$$c_3(\xi,t) = 0, \tag{C.3}$$

$$a(\xi,t) = \frac{k}{\gamma_w}\frac{1}{(\tilde{C}_1 C_{3311} + \tilde{C}_3 C_{3322} + C_{3333})}, \tag{C.4}$$

$$b_1(\xi,t) = 2\frac{(\tilde{C}_2 C_{3311} + \tilde{C}_4 C_{3322} + C_{3313})}{(\tilde{C}_1 C_{3311} + \tilde{C}_3 C_{3322} + C_{3333})}, \tag{C.5}$$

$$b_2(\xi,t) = 0, \tag{C.6}$$

where

$$\tilde{C}_1 = \frac{(C_{1122}C_{2233} - C_{1133}C_{2222})}{(C_{2222}C_{1111} - C_{2211}C_{1122})}, \tag{C.7}$$

$$\tilde{C}_2 = \frac{(C_{1122}C_{2213} - C_{1113}C_{2222})}{(C_{2222}C_{1111} - C_{2211}C_{1122})}, \tag{C.8}$$

$$\tilde{C}_3 = \frac{(C_{1133}C_{2211} - C_{2233}C_{1111})}{(C_{2222}C_{1111} - C_{2211}C_{1122})}, \tag{C.9}$$

$$\tilde{C}_4 = \frac{(C_{2211}C_{1113} - C_{1111}C_{2213})}{(C_{2222}C_{1111} - C_{2211}C_{1122})}. \tag{C.10}$$

Appendix D

In the elasto-viscoplastic case, the coefficients of Eqs. (8a)–(8c) become (in all the following definitions, it is very important to underline, C_{ijhk} must be read as C^{el}_{ijhk}):

$$c_1(\xi,t) = -2(\tilde{C}_1 C_{1311} + \tilde{C}_3 C_{1322} + C_{1333}), \tag{D.1}$$

$$c_2(\xi,t) = 4(\tilde{C}_2 C_{1311} + \tilde{C}_4 C_{1322} + C_{1313}), \tag{D.2}$$

$$c_3(\xi,t) = 2(\tilde{C}_{M1} C_{1311} + \tilde{C}_{M2} C_{1322} + M_4), \tag{D.3}$$

$$a(\xi,t) = \frac{k}{\gamma_w} \frac{1}{(\tilde{C}_1 C_{3311} + \tilde{C}_3 C_{3322} + C_{3333})}, \tag{D.4}$$

$$b_1(\xi,t) = 2\frac{(\tilde{C}_2 C_{3311} + \tilde{C}_4 C_{3322} + C_{3313})}{(\tilde{C}_1 C_{3311} + \tilde{C}_3 C_{3322} + C_{3333})}, \tag{D.5}$$

$$b_2(\xi,t) = \frac{(\tilde{C}_{M1} C_{3311} + \tilde{C}_{M2} C_{3322} + M_3)}{(\tilde{C}_1 C_{3311} + \tilde{C}_3 C_{3322} + C_{3333})}, \tag{D.6}$$

where

$$\tilde{C}_1 = \frac{(C_{1122}C_{2233} - C_{1133}C_{2222})}{(C_{2222}C_{1111} - C_{2211}C_{1122})}, \tag{D.7}$$

$$\tilde{C}_2 = \frac{(C_{1122}C_{2213} - C_{1113}C_{2222})}{(C_{2222}C_{1111} - C_{2211}C_{1122})}, \tag{D.8}$$

$$\tilde{C}_3 = \frac{(C_{1133}C_{2211} - C_{2233}C_{1111})}{(C_{2222}C_{1111} - C_{2211}C_{1122})}, \tag{D.9}$$

$$\tilde{C}_4 = \frac{(C_{2211}C_{1113} - C_{1111}C_{2213})}{(C_{2222}C_{1111} - C_{2211}C_{1122})}, \tag{D.10}$$

$$\tilde{C}_{M1} = \frac{(C_{1122}M_2 - C_{2222}M_1)}{(C_{2222}C_{1111} - C_{2211}C_{1122})}, \tag{D.11}$$

$$\tilde{C}_{M2} = \frac{(C_{2211}M_1 - C_{1111}M_2)}{(C_{2222}C_{1111} - C_{2211}C_{1122})}, \tag{D.12}$$

$$\begin{array}{l} M_1 = \dot{\varepsilon}_{11}^{\mathrm{vp}}; M_2 = \dot{\varepsilon}_{22}^{\mathrm{vp}}; \\ M_3 = \dot{\varepsilon}_{33}^{\mathrm{vp}}; M_4 = \dot{\varepsilon}_{13}^{\mathrm{vp}}. \end{array} \tag{D.13}$$

Appendix E

In the following two tables are reported (Tables 1 and 2). In the first one the constitutive parameters calibrated on the mechanical response of a very dense Hostun RF sand ($D_r = 100\%$) are collected, in the second one those calibrated on the mechanical behaviour of a very lose Hostun RF sand ($D_r = 20\%$). As previously clarified (Appendix B), the only index to be assigned is the initial relative density. In the following, the initial relative density (D_{r0}) is 20 %.

Table 1
Constitutive parameters for dense Hostun RF sand

Elastic parameters	B_0 (kPa)	RF	α_c
$D_r = 100\%$	1528	0.28	0.25
Plastic parameters	γ	B_p (kPa)	t_p
$D_r = 100\%$	3.4	0.002	10
	$\hat{\beta}_f$	ξ_e	ξ_c
	0.5	−0.24	−0.09
	c_p	$\hat{\theta}_e$	$\hat{\theta}_c$
	38.0	0.218	0.42
Viscous parameters	α	$\bar{\gamma}$	
$D_r = 100\%$	61	0.000002	

Table 2
Constitutive parameters for loose Hostun RF sand

Elastic parameters	B_0 (kPa)	RF	α_c
$D_r = 20\%$	1028	0.28	0.25
Plastic parameters	γ	B_p (kPa)	t_p
$D_r = 20\%$	3.7	0.0049	10
	$\hat{\beta}_f$	ξ_e	ξ_c
	0.5	−0.1178	−0.2585
	c_p	$\hat{\theta}_e$	$\hat{\theta}_c$
	18	0.1184	0.253
Viscous parameters	α	$\bar{\gamma}$	
$D_r = 20\%$	61	0.0000002	

References

Andersen, A., Bjerrum, L., 1968. Slides in subaqueous slopes in loose sand and silt. Norwegian Geotechnical Institute, no. 81, pp. 1–9.

Canou, J., Thorel, L., De Laure, E., 1991. Influence d'un déviateur de contrainte initial sue les caracté ristiques de liqué faction statique du sable. Proc. X ECSMFE, Firenze, vol. 1, pp. 49–52.

Castro, G., 1969. Liquefaction of sands. Ph.D. Thesis, Harvard University, Cambridge, Massachusetts.

di Prisco, C., Imposimato, S., 1996. Time dependent mechanical behaviour of loose sand. Mechanics of Cohesive-Frictional Materials 1 (1), 45–73.

di Prisco, C., Imposimato, S., in press. Non Local numerical analyses of strain localisation in dense sand. Mathematical and Computer Modelling.

di Prisco, C., Pastor, M., 2000. Constitutive equations in plasticity. In: Cambou, B., di Prisco, C. (Eds.), Constitutive Modelling of Geomatérials, Rev. Franç. Geotech. 4, no. 5/2000, Hermes editor.

di Prisco, C., Nova, R., Lanier, J., 1993. A mixed isotropic-kinematic hardening constitutive law for sand. In: Kolymbas, D. (Ed.), Modern Approaches to Plasticity, pp. 83–124.

di Prisco, C., Matiotti, R., Nova, R., 1995. Theoretical investigation of the undrained stability of shallow submerged slopes. Géotechnique 45 (3), 479–496.

di Prisco, C., Imposimato, S., Nova, R., 1999. Sand specimen undrained mechanical response to instantaneous load increments. Proceedings of the Seventh International Symposium Plasticity'99 on Constitutive and Damage Modelling of Inelastic Deformation and Phase Transformation—Cancun 5–13 January 1999, pp. 557–560.

di Prisco, C., Mancinelli, L., Zanelotti, L., in press. Rapid sedimentation: a triggering factor for liquefaction of submerged slopes. Mechanics of Cohesive-Frictional Materials.

Ishihara, K., 1993. Liquefaction and flow failure during earthquakes. Géotechnique 43 (3), 351–415.

Lade, P.V., 1992. Static instability and liquefaction of loose fine sandy slopes. J. Geot. Engrg., ASCE 118 (1), 51–71.

Lade, P.V., Nelson, R.B., 1987. Modelling the elastic behaviour of granular materials. Int. J. Numr. Anal. Meth. Geomech. 11 (5), 521–542.

Lanier, J., di Prisco, C., Nova, R., 1991. Etude experimentale et analyse théorique de l' anisotropie induite du sable d' Hostun. Rev. Franç. Geotech. 57, 59–74.

Kramer, S.L., Seed, H.B., 1988. Initiation of soil liquefaction under static loading condition. J. Geot. Engrg., ASCE 114 (4), 412–430.

Nova, R., 1988. Sinfonietta classica: an exercise on classical soil modelling. In: Saada, A., Bianchini, G. (Eds.), Proceedings of the Symposium on Constitutive Equations for Granular non-cohesive soils, Cleaveland, pp. 501–520.

Nova, R., 1991. A note on sand liquefaction and soil stability. Proceedings of the Third International Conference on Constitutive Laws for Engineering Materials, Tucson, pp. 153–156.

Perzyna, P., 1963. The constitutive equations for rate sensitive plastic materials. Quart. Appl. Math. 20, 321–332.

Sladen, J.A., D'Hollander, R.D., Krahn, J., 1985. The liquefaction of sands, a collapse surface approach. Can. Geotech. J. 22, 564–578.

Terzaghi, K., 1957. Varieties of submarine slope failure. Norwegian Geotechnical Institute, Publication no. 25, pp. 1–16.

Vardoulakis, I., Stavropoulos, M., Skjaerstein, A., 1998. Porosity waves in a fluidized sand-column test. Phil. Trans. Royal Soc. Lond. A. 356, 2591–2608.